Available online at www.pelagiaresearchlibrary.com

Pelagia Research Library

Der Chemica Sinica, 2017, 8(6):513-523

ISSN : 0976-8505
CODEN (USA): CSHIA5

Improving the Corrosion Behavior of Ductile Cast Iron in Sulphuric Acid by Heat Treatment

TFH Mohamed, SS Abd El Rehim and MAM Ibrahim*

Chemistry Department, Faculty of Science, Ain Shams University, Abbassia, Cairo, Egypt

ABSTRACT

In this investigation, the effect of heat treatment on the corrosion behavior of ductile cast iron (DCI) in H_2SO_4 environment has been conducted. Moreover, the effect of heat treatment on the mechanical properties has also been investigated. The change in microstructure of DCI is obtained by austenetising at 900°C for two hours followed by oil quenching and then heated to 700°C for different tempering times. The corrosion measurements were tested using anodic potentiodynamic polarization and cyclic polarization techniques. Here we show that the tempered specimens at different tempering times show better corrosion resistance in H_2SO_4 solution than that without heat treatment. Moreover, the polarization measurements showed that the E_{corr} and i_a of the different specimens increase with increasing H_2SO_4 concentration while both E_{pass} and i_{pass} were decreased.

Keywords: Ductile cast iron, Corrosion behaviour, Potentiodynamic, Cyclic polarization, Heat treatment

INTRODUCTION

Ductile cast iron (DCI) possesses several engineering and manufacturing advantages when compared with cast steels [1,2]. These include an excellent damping capacity, better wear resistance, 20-40% lower manufacturing cost and lower volume shrinkage during solidification [3,4]. The combination between the good mechanical properties and the casting abilities of DCI makes its usage successful in structural applications especially in the automotive industry. However, DCI suffers corrosion because of the free graphite content (2-4% by weight); an insoluble graphitic layer of corrosion products is left behind in the process of corrosion [5-7]. These corrosion products are very dense, adherent, have considerable strength, and form a barrier against further corrosion. In comparison with steel corrosion, because of the absence of free graphite in steel, the corrosion products have little or no strength or adherence and flake off as they are formed, thus presenting fresh surfaces for further corrosion.

However, the corrosion behaviour of DCI in aqueous environments has little attention [8-10]. While much is known about the effect of alloying elements on the mechanical properties of cast irons, little is probably known about the effect of heat treatment on their corrosion behaviour [11]. The corrosion resistance of DCI is related to its microstructure which is determined by heat treatment parameters (austenitising temperature and time). Therefore, the aim of this research is to shed light on the effect of heat treatment on the corrosion behavior of DCI in H_2SO_4 environment and to throw more light on their microstructure and mechanical properties.

MATERIALS AND METHODS

The specimens of DCI were supplied locally by Delta Steel Mill Company, Egypt. The specimens were casted according to the procedure recommended by ASTM [12] and were machined in the form of rods (~ 6.5 mm diameter and 7 cm length) for polarization measurements. However, for strength and hardness tests, the specimens were formed with dimensions given in ASTM [13]. The chemical composition of the specimens used was determined using emission spectroscopic technique with the aid of ARL quant-meter (model 31000-292 IC). The chemical composition of the cast iron used in the present work contains: C= 3.61%, Si = 2.65%, Mn = 0.45%, S% = 0.015%, P = 0.025%, Mg = 0.06% and Fe is the remaining. The specimens were mechanically polished by emery paper No. 1000 and chemically

etched using Nital (3% nitric acid in methanol).

Heat treatment of cast iron was carried out in an electrical muffle furnace. Charcoal was placed around the specimens to avoid oxidation. Quenching and tempering cycle was used. Oil quenching was applied after austenitising (900°C for two hours). Quenched specimens were then tempered at 700°C for different tempering times. The following six specimens were prepared as following: specimen No. 0 was obtained without heat treatment (as received DCI). Specimen No. 1 was obtained after the first stage of the cycle (after ausenitising at 900°C for two hours and then quenched in oil). The second stage of heat treatment was achieved by reheating the oil quenched specimens at 700°C for different holding times: 10, 15, 30 and 60 minutes, respectively before air cooling to room temperature corresponding to specimens Nos. 2-5.

Microstructure changes in the heat-treated specimens were characterized by using optical microscope technique. Tensile strength of specimen's Nos. 0-5 was determined according to ASTM standard SHIMADZU machine (Model UMH-20 Kyato-Japan). Brinel hardness was measured on the specimens before and after heat treatment using SHIMADZU machine. The electrochemical measurements were carried out in three-electrode cell by using a computer assisted potentiostat (EG&G PAR 273). A platinum wire was used as the counter electrode. The specimen of DCI was used as the working electrode. The reference electrode used was a saturated calomel electrode (SCE). All the electrolyte solutions were prepared from analytical grade chemical reagents and were used without further purifications. All solutions were freshly prepared using doubly distilled water. The corrosion behavior of DCI was investigated in H_2SO_4 solution. Potentiodynamic polarization measurements were carried out by sweeping the potential starting from -1500 to 2000 mV with scan rate of 100 mVs^{-1}. The polarization curves were recorded by changing the electrode potential automatically from the starting potential towards more positive direction with required scan rate. The cyclic voltammetry was carried out in the potential range -1000 to -1500 mV. In all cases, duplicate experiments were carried out to ensure reproducibility. The composition and structure of the passive film formed on some specimens were examined by a Philips XRD Model No. 1730 (40 kV), Ni filter and CuK_{α} radiation. The scanning speed was 1.0º per minute.

RESULTS AND DISCUSSION

Microstructure and mechanical properties of DCI

The microstructure of specimens (0-5) was examined using optical microscope. The micrographs of the polished and chemically etched specimens are given in **Figure 1 (a-f)**, and the percentage of different phases is included in **Table 1**.

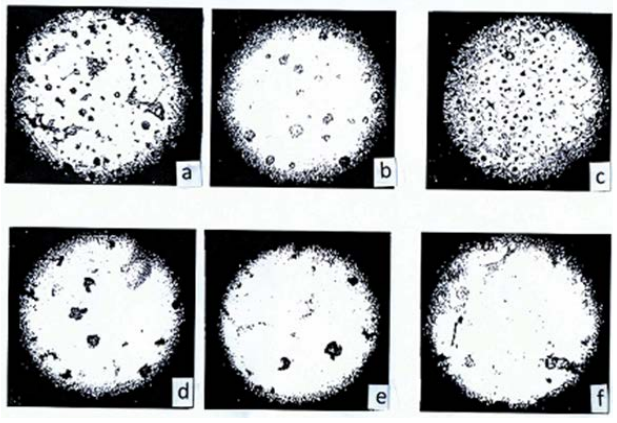

Figure 1: Microstructure of the different specimens etched with 2% Nital; specimen No. 0 shows the pearlitic structure (a), specimen No.1 shows the martensitic structure (b), specimen No.2 shows the martensitic-ferritic structure (c), specimen No.3 shows the pearlitic structure (d), specimen No. 4 shows the ferritic-martensitic (e), and specimen No. 5 shows the ferritic-martensitic structure (f), 200X.

The data show that the microstructure of the as received DCI (specimen No. 0) contained ferrite and pearlite matrix (**Figure 1a**). The ferrite content is about 80% of the matrix. Small percentage of graphite (3.0%) is present as balls or spherulites rather than as flacks (primary graphite). The spherulite graphite is dispersed in ferrite matrix. On heating the as received DCI to 900°C for two hours, austenite structure was retained. However, after oil quenching, the austenite

phase transformed completely to martensite (specimen No.1) as shown in **Figure 1b**. The martensite phase is a supersaturated solid solution of carbon in iron which has a body-centered tetragonal crystal structure [14]. Martensite forms austenite by slight rearrangement of iron atoms required to transform the face centered crystal structure into body-centered tetragonal structure. Tempering the oil quenched martensite (specimen No.1) was achieved by reheating the sample to 700°C for different tempering times.

Specimen's Nos. 2-5, was obtained after tempering times of 10, 15, 30 and 60 minutes at 700°C, respectively, before air cooling to the room temperature 30°C. The data obtained reveal that, on tempering martensite, the carbon tended to precipitate out of the solid solution as carbides (FeC_3) and breakdown of the carbides into ferrite and graphite (secondary graphite) $FeC_3 \rightarrow$ Fe (ferrite)+3C. The effect of tempering time on the microstructure is illustrated in **Figure 1(a-f)** and **Table 1**. The percentage of ferrite increases with increasing the tempering time. Nearly complete fertilization was achieved after one-hour tempering time. The secondary graphite particles are closely distinguished in **Figure 1**, where complete graphitization of the precipitated carbides had occurred.

Table 1: Different phases of specimen's Nos. 0-5, the hardness, tensile strength of the DCI, and the values of the activation energy (E).

Specimen No.	Phase%				Brinel Hardness	Tensile Strength kg mm^{-2}	Activation energy kJ mol^{-1}
	Free graphite	Ferrite	Pearlite	Martensite			
0	3	80	17	-	187	64	17.2
1	3	-	-	97	492	120	25.8
2	3	5	-	92	341	117	18.5
3	3	16	-	81	282	98	19.3
4	3	77	-	20	176	62	20.7
5	3	92	-	5	170	58	21.1

On the other hand, the effect of heat treatment on the measured hardness of the as received-DCI as well as on the heat- treated specimens, is summarized in **Table 1**. The data reveal that the hardness of the martensite (specimen No.1) is much higher than the hardness of the as-received DCI (specimen No. 0) (which consists mainly of ferrite and pearlite). The increase in the hardness is probably due partly to the strain involved in retaining the carbon in solid solution in body-centered tetragonal iron and partly to their very high dislocation density [14]. However, tempering the martensite specimen at 700°C caused a decrease in the hardness. The decrease in the hardness is directly proportional to the tempering time.

However, the effect of heat treatment on tensile strength of the specimens was determined and the values of tensile strength are included in **Table 1**. It was observed that, the tensile strength of martensite (specimen No. 1) is higher than that of the as received cast iron (specimen No. 0). However, on tempering the martensite specimens, the tensile strength tended to decrease in proportion to the tempering time. These results can be interpreted based on increasing the percentage of ferrite phase in the specimens. Generally, tensile strength is greater in pearlitic irons than in ferritic irons.

Corrosion behaviour of DCI in H_2SO_4 solution

The anodic potentiodynamic polarization curves of DCI in H_2SO_4 solution was carried out under different conditions of acid concentration, scan rate and temperature. **Figures 2 and 3** illustrate the anodic potentiodynamic E-i curves of the as-received DCI (specimen No. 0) and the heat- treated specimen's (Nos. 1-5) in 1.0 M and 2.0 M H_2SO_4 respectively at 30°C. It was found that, the heat treatment as well as the change in acid concentration has no significant influence on the general features of the polarization curves. Inspections of these curves reveal that: on positive going scan, cathodic current densities, i_c corresponding to hydrogen evolution reaction decreases gradually and reach zero values at E_{corr} (zero current potential). However, the anodic parts of the curves are complicated, and each curve exhibits an active to passive transition state. In the active dissolution region, the anodic current density i_a corresponding to the anodic dissolution of Fe, increases exponentially with the applied potential according to the following equation:

$$i_a = K\, e^{(\alpha zFE/RT)} \quad (1)$$

where, K is the rate constant, α is the transfer coefficient, E is the anodic potential, z is the number of electrons and F is the Faraday's constant. The active region is followed by a narrow limiting current region associated with current oscillations. At certain potential (passivation potential), E_{pass}, the anodic current drops to a very small current value

i_{pass} indicating the onset of permanent passivation. In E-i curves, the height of the anodic dissolution current before the current oscillation region represents the critical current density i_p. Current oscillation phenomenon is usually observed during the anodic electro dissolution-passivation of iron and steel in sulphuric acid solutions [15].

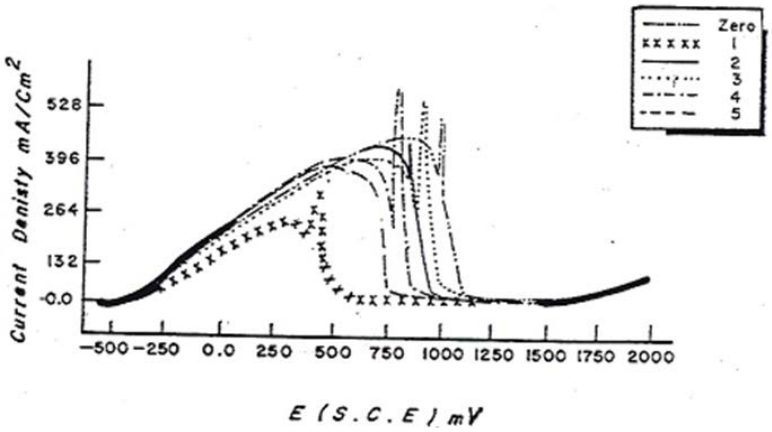

Figure 2: Potentiodynamic anodic polarization curves for the six specimens in 1.0 M H_2SO_4 at 30°C and at scan rate of 100 mVs^{-1}.

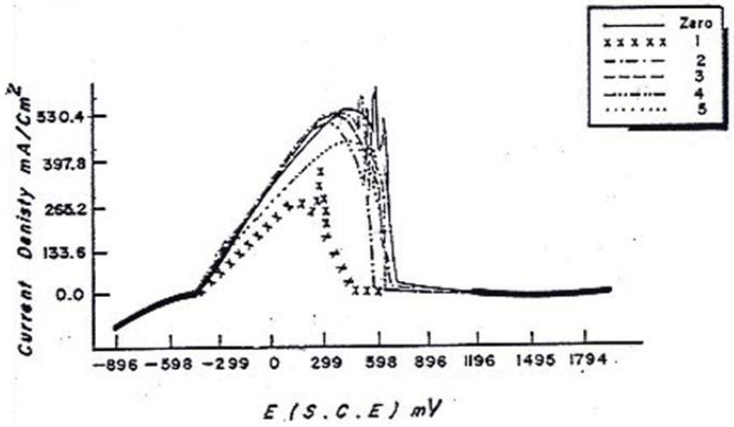

Figure 3: Potentiodynamic anodic polarization curves for the six specimens in 2.0 M H_2SO_4 at 30°C and at scan rate of 100 mVs^{-1}.

Many theories have been suggested to explain the oscillation phenomenon [16-21]. Several authors showed that the iR_s potential is dropped (where R_s, is the solution uncompensated resistance) and mass transport might induce oscillations of the Fe/H_2SO_4 system. However, Russell et al. [20] demonstrated that, the oscillatory behaviour of Fe/H_2SO_4 before passivation is associated with cyclic formation, growth and dissolution of $FeSO_4$ salt film on the electrode surface. Wang et al. [22], on using a halographic microphotographic technique at the Fe/H_2SO_4 interface suggest temporal formation of $Fe(OH)_2$ and/ or Fe_3O_4 in acidic media can be given by considering the local decrease of H^+ concentration. This is due to migration of H^+ when Fe^{2+} accumulates under the Fe electrode. The local increase of pH leads to a temporal precipitation of $Fe(OH)_2$ or Fe_3O_4 and blocking of the Fe surface. The $Fe(OH)_2$ and Fe_3O_4 remain stable for a while but are dissolved when H^+ concentration increase locally due to the backward diffusion of H^+ from the bulk of the solution. The oscillation of H^+ concentration is also the basic principle of the model formulated by Frank [23] to describe the current oscillations. This periodic blocking and activation ceases at more positive potentials where a stable passive oxide (γ-Fe_2O_3) is formed [24]. The passive region extends up to oxygen evolution potential at which the current density increases sharply. X-ray diffraction analysis on the surface of the as received-DCI electrode passivated potentiodynamically up to oxygen evolution potential in 1.0 M H_2SO_4 showed that the passivity is due to the formation of Fe_2O_3 film on the electrode surface.

It can also be seen from **Figures 2** and **3** that the anodic current densities in both the active and passive regions and hence the anodic dissolution rate of specimen No. 0 in H_2SO_4 are the highest while its corresponding passive potential, E_{pass} has the most positive potential value. The pearlitic structure of this specimen consists of alternate plates or lamellar of cementite and ferrite (**Table 1**). In addition to the graphite spherulites, the cementite plates acting as

cathodes, offer large interface areas with adjoining anodic ferrite plates. The existence of such local couples enhances the rate of anodic dissolution. However, the oil quenched martensite specimen (specimen No. 1) show the lowest rate of corrosion. This observation is because the martensite consisted of one phase. Carbon atoms randomly occupy the interstitial sites of the body-centered tetragonal lattice, and are electronically interacted with the neighboring iron atoms. This can limit their effectiveness as cathodes as local-action cells and thus reduces the corrosion rate of the specimen. On the other hand, tempering the oil quenched martensite at 700°C (specimen's Nos. 2-5) enhances their corrosion rates. This enhancement is due to the microstructure changes occurred on tempering. Carbide precipitation and its breakdown into graphite and ferrite were observed on tempering at 700°C. These processes increase the heterogeneity of the matrix and hence enhance the corrosion. The rate of corrosion decreases with increasing the tempering time. Therefore, we can conclude that the tempered specimens at different tempering times show better corrosion resistance than that without heat treatment (as-received).

The effect of the H_2SO_4 concentrations (0.5-2.0 M) on the polarization response of the as-received cast iron and the heat-treated specimens was studied. As mentioned above the acid concentration has no significant change on the general shape of the polarization curves, therefore, the data is not included here. However, the results reveal that the zero-current potential E_{corr} and the anodic current density i_a of the different specimens increase with increasing the acid concentration from 0.5 to 2.0 M at 30°C. **Figure 4** illustrates the linear relation between i_p and log acid concentration.

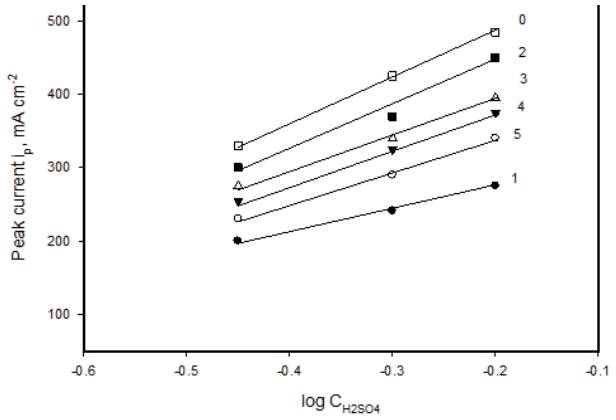

Figure 4: Dependence of i_p on logC_{H2SO4}.

On the other hand, the effect of scan rate υ on the polarization curves of the specimen's Nos. 0-5 in 1.0 M H_2SO_4 and at 30°C was evaluated as shown in **Figure 5**. In all cases, it is observed that an increase in the scan rate enhances the anodic dissolution of the specimens and delays the attainment of passivity. Both, the peak potential, E_p and peak current, i_p increase with increasing the scan rate. The linear relationship between E_p vs log υ is shown in **Figure 6**. These data could be explained on the basis that the time allowed to nucleate (or growth) of iron oxide crystals at its equilibrium potential is very short, and passivation is delayed until the nuclei have grown to the critical size required for passivation [25]. On the other hand, the relation between the peak current i_p and the square root of scan rate is shown in **Figure 7**. The linear relation between peak current i_p vs $\upsilon^{1/2}$ indicates diffusion controlled process (limitation of the film formation).

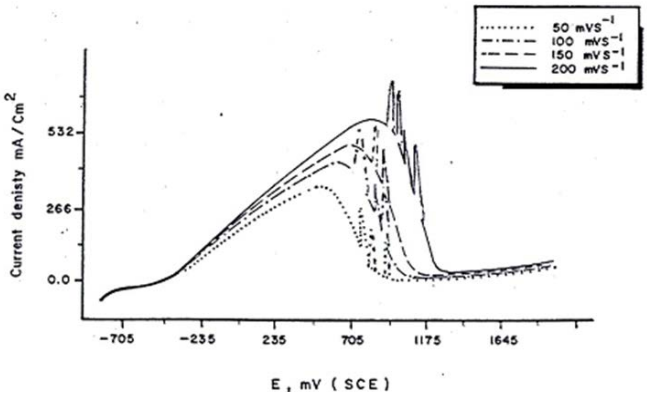

Figure 5: Potentiodynamic anodic polarization curves for specimen No. 0 in 2.0 M H_2SO_4 at 30°C and at different scan rates.

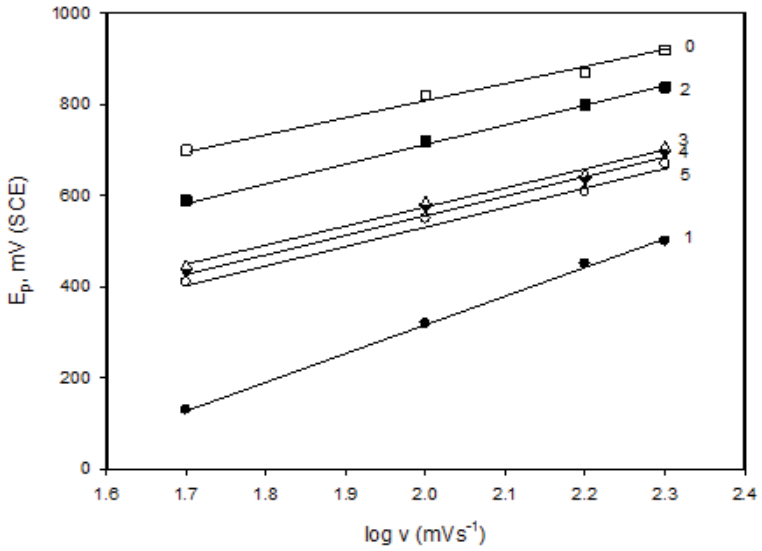

Figure 6: Dependence of E_p on log υ.

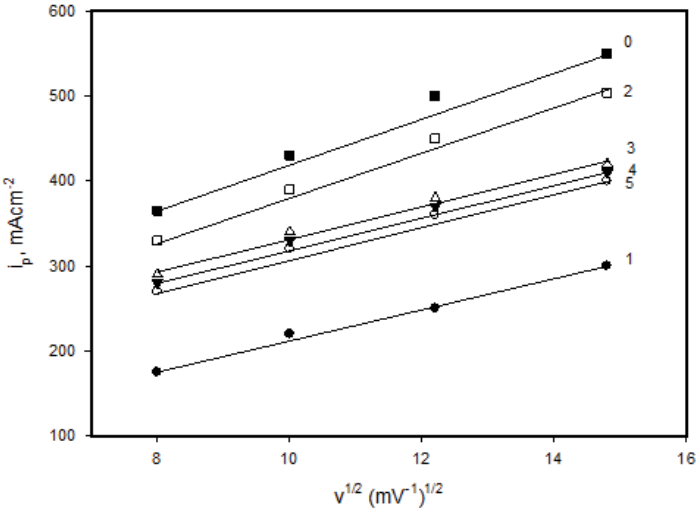

Figure 7: The relationship between i_p versus $\upsilon^{1/2}$.

The effect of solution temperature on the polarization profiles of the six specimens (0-5) in 1.0 M H_2SO_4 has been studied over the temperature range from 30-70°C. The results are given in **Figure 8 (a-c)**. An increase of solution temperature increases the active dissolution and delays the passivation. At temperature higher than 40°C, the anodic current density i_a for the specimens except specimen No. 1 increases exponentially with the applied potential up to 2000 mV without any sign for passivity. At 70°C, no passive region was observed for all the six specimens (**Figure 8c**). It is known that for the same metal, under similar conditions, the value of i_a (at a given potential) may be taken to be proportional with the rate of corrosion. **Figure 9** shows log i_a (at E= 700 mV) plotted against the reciprocal of the absolute temperature (1/T) for the specimen No. 0 as an example and the results are shown to be linear for all specimens which can be expressed by Arrhenius equation:

$$\log i_a = A-(E^* / 2.303\ RT) \quad (2)$$

Where E* represents the apparent activation energy, the values were determined from the slopes of the straight lines. **Table 1** includes the value of the apparent activation energy for each specimen.

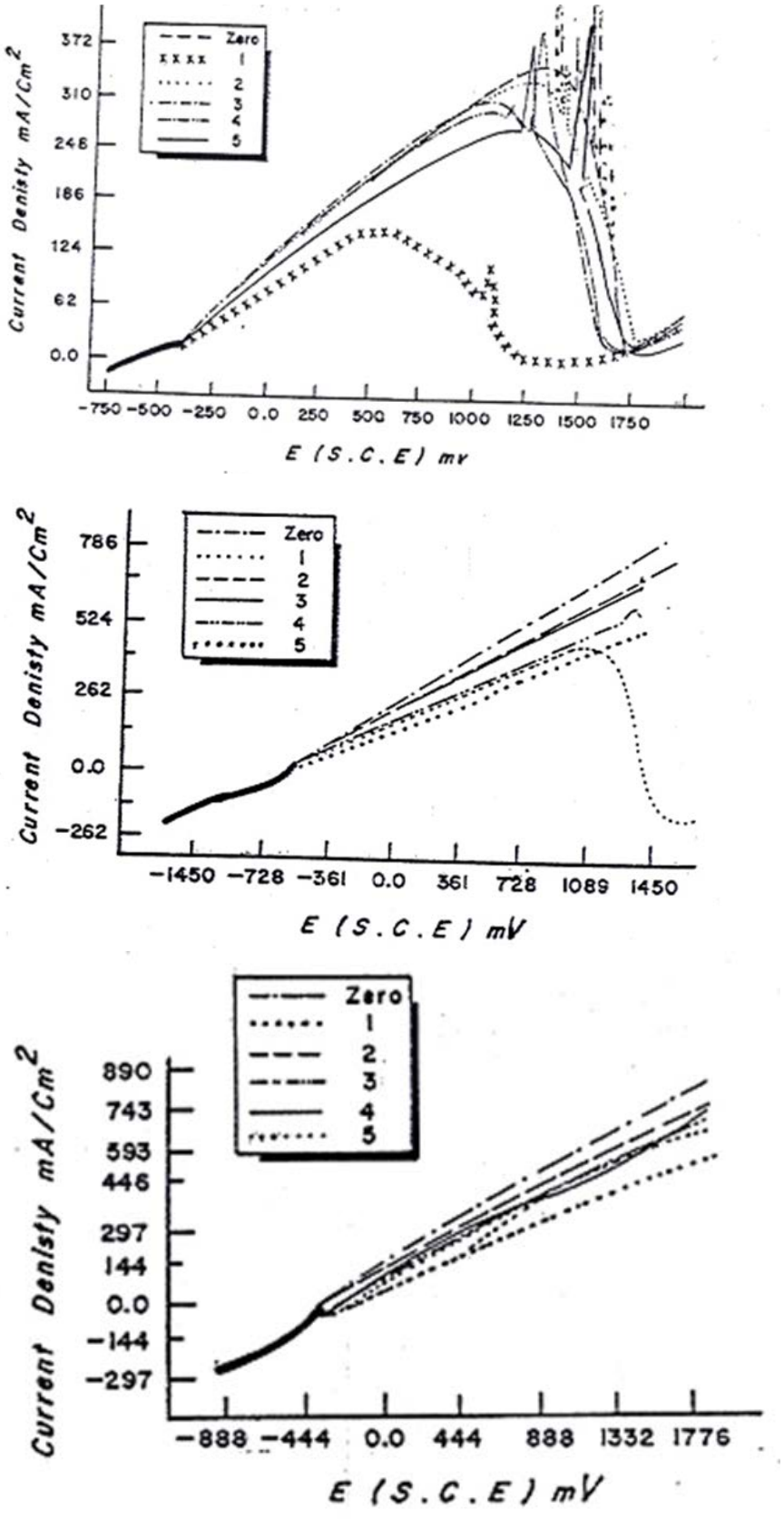

Figure 8: Potentiodynamic polarization curves for the six specimens in 0.5 M H_2SO_4, scan rate 100 mVs^{-1} at 40°C (a), at 60°C (b), and at 70°C (c).

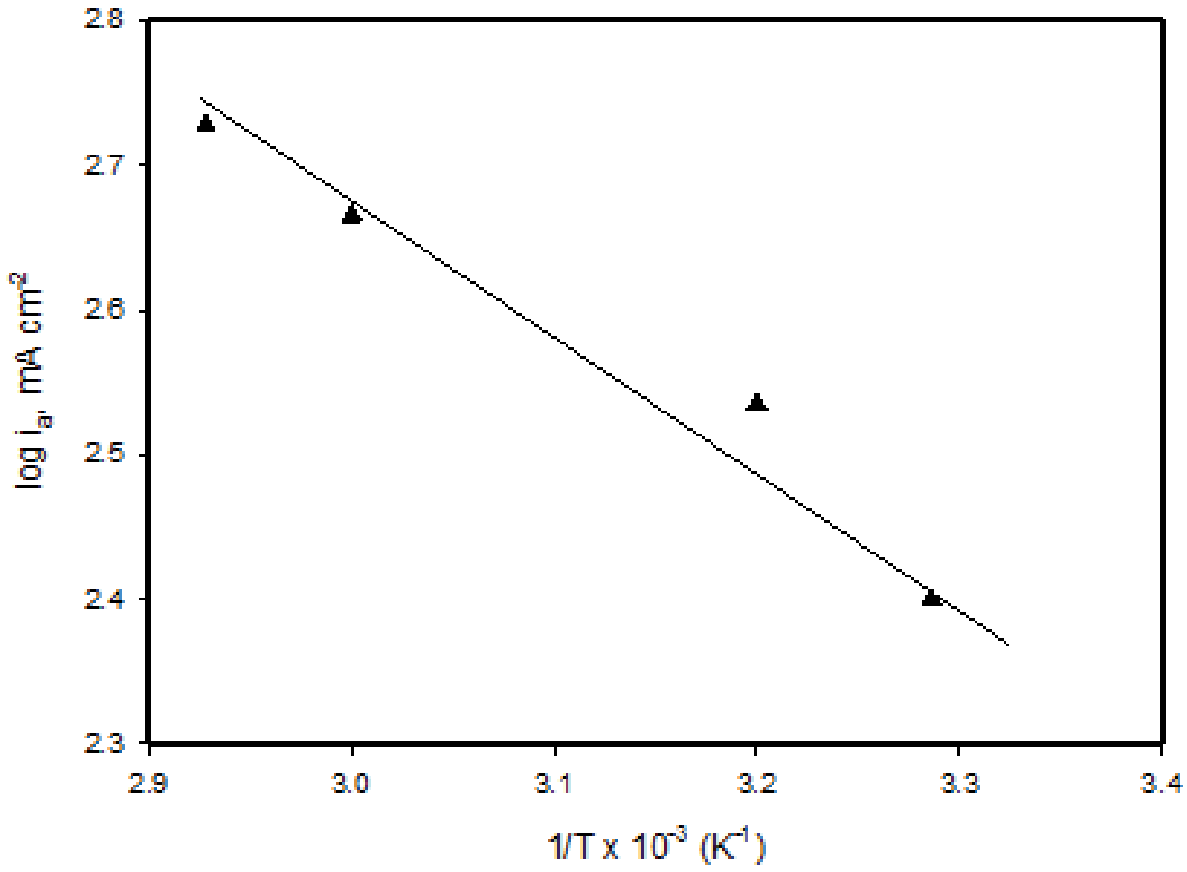

Figure 9: Dependence of log i_p on (1/T), $(^oK)^{-1}$ for specimen No. 0 in 0.5 M H_2SO_4 solution at scan rate of 100 mVs^{-1} and at E=700 mV.

Cyclic polarization

To throw more light on the effect of heat treatment on the electrochemical response of DCI, cyclic polarization measurements were performed [26] as shown in **Figure 10 (a-c)**. It illustrates cyclic polarization of specimen No. 0 in 1.0 M H_2SO_4 at 30°C and at scan rate of 100 mVs^{-1}. The cyclic polarization started from -1500 mV and was reversed at various anodic potential limits. Inspections of these results show that if the anodic potential is reversed at the ascending branch of the active dissolution region (**Figure 10a**), the reverse scan retraces itself. On the other hand, if the anodic potential is reversed within the oscillatory region (**Figure 10b**), hysteresis loop between the forward and reverse scan is observed. However, if the anodic potential is reversed within the passive region (**Figure 10c**) the reverse passive current is usually smaller than the forward passive current. This reversal passive current remains nearly constant up to a certain critical potential E_r within the active dissolution peak AI at which the anodic current i_a increases suddenly and rapidly forming a reactivation anodic dissolution peak AII. The appearance of this reaction peak AII might be assigned to removal of the passive layer and oxidation of iron through defects and cracks of the passive layer [27]. The reactivation potential E_r is the minimum anodic potential for passivation to occur. On the other hand, the appearance of peak AII could be assigned to the oxidation of underlying iron as shown in boric-borate solution [28]. It is observed that for all specimens the quantity of electricity consumed within peak AI is always larger than that consumed in peak AII for all the specimens. Similar results were obtained for specimen's Nos. 1-5.

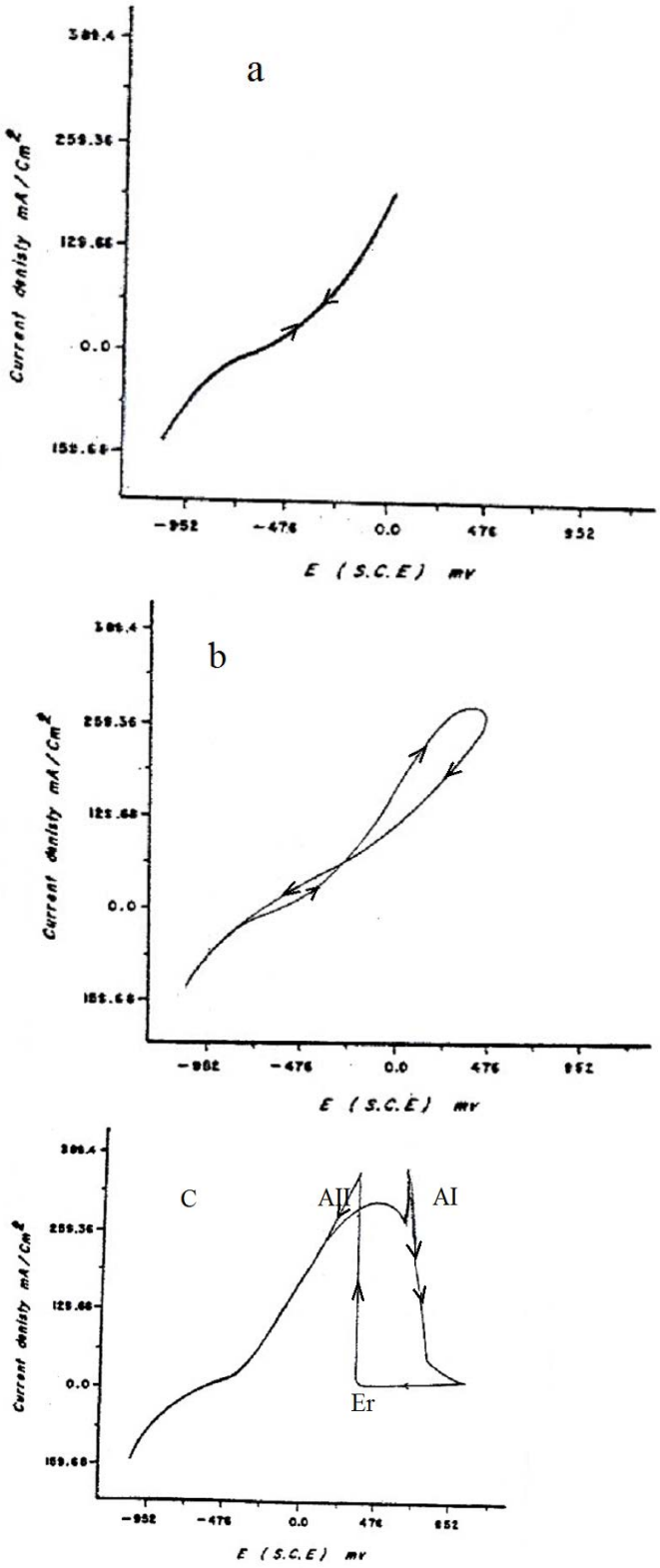

Figure 10: Typical cyclic polarization curves for specimen No. 0 in 1.0 M H_2SO_4 at 30°C and at scan rate of 100 mVs^{-1} starting from -1500 and reversed at various anodic potentials: a) from -1500 to 0 mV, b) From -1500 to 470 mV, c) from -1500 to 1000 mV.

CONCLUSION

The effect of heat treatment on the corrosion behaviour of ductile cast iron (DCI) in H_2SO_4 environment has been

conducted. In addition, the effect of heat treatment on the mechanical properties has also been conducted. Here we find that the tempered specimens at different tempering times show better corrosion resistance in H_2SO_4 solution than that without heat treatment. The tensile strength of martensite (specimen No. 1) is much higher than that of the cast iron (specimen No. 0). However, on tempering the martensite specimens, the tensile strength tended to decrease in proportion to the tempering time. Moreover, the electrochemical measurements show that the E_{corr} and i_a of the different specimens increase with increasing the acid concentration while both E_{pass} and i_{pass} were decreased. The values of i_{corr}, indicates the accelerating influence of rising solution temperature on the corrosion of DCI. Furthermore, the pitting potential E_{pit} becomes less noble with increasing solution temperature and with decreasing the scan rate.

REFERENCES

[1] Sedriks AJ (**1996**) Corrosion of stainless steels. 2nd edn., Wiley-Interscience, New York, USA.

[2] Smart NR, Blackwood DJ, Werme L (**2002**) Anaerobic corrosion of carbon steel and cast iron in artificial groundwaters: Part 1-electrochemical aspects. *Corrosion* 58: 547-559.

[3] Jones DA (**1996**) Principles and Prevention of Corrosion. 2nd edn., Prentice Hall, Upper Saddle River, New Jersey, US.

[4] Kenawy MA, Abdel-Fattah A, Okasha N, EL-Gazery M (**2001**) Mechanical and Structural Properties of Ductile Cast Iron. *Egypt J Sol* 24: 75-84.

[5] Olawale JO, Odusote JK, Rabiu AB, Ochapa EO (**2013**) Evaluation of corrosion behaviour of grey cast iron and low alloy steel in cocoa liquor and well water. *Sci Res* 1: 44-48.

[6] Bahrin EK, Baharuddin AS, Ibrahim MF, Razak MNA, Sulaiman A, et al. (**2009**) Physicochemical property changes and enzymatic hydrolysis enhancement of oil palm empty fruit bunches treated with superheated steam. *Bio Resource* 7: 1784-1801.

[7] Aramide FO, Olorunniwo EO, Atanda PO, Borode JO (**2010**) Corrosion characteristics of ascast ductile iron in lime juice. *JMMCE* 9: 867.

[8] Mehra R, Soni A (**2002**) Cast iron deterioration with time in various aqueous salt solutions. *Bull Mater Sci* 25: 53-58.

[9] Smart NR, Blackwood DJ, Werme L (**2002**) Anaerobic corrosion of carbon steel and cast iron in artificial groundwaters: Part 2-gas generation. *Corrosion* 58: 627-637.

[10] Jayaraman TV, Srisuukhumbowornchai N, Guruswamy S, Free ML (**2007**) Corrosion studies of single crystals of iron-gallium alloys in aqueous environments. *Corros Sci* 49: 4015-4027.

[11] Fathy N (**2013**) Influence of semi-solid isothermal heat treatment on microstructure of gray cast iron. *JMMCE* 1: 326.

[12] ASTM (**1964**) Canada center for mineral and energy technology.

[13] Annual book of ASTM standard, E8-79.

[14] Brick RM, Philips AL (**1966**) Structure and properties of alloys. 3rd edn., Eurasia publishing house, New Delhi, India.

[15] Ferhat M, Benechattara A, Amara SE, Najjar D (**2014**) Corrosion behaviour of Fe-C alloys in a Sulfuric Medium. *J Mater Environ Sci* 5: 1059-1068.

[16] Lorbeer P, Lorenz WJ (**1983**) Active-passive transition of metals. *Werkst Korros* 34: 290-294.

[17] Kado T, Munitmi N (**1991**) A model for the current oscillations of iron in sulfuric acid. *J Electrochem Soc* 138: 3312-3321.

[18] Rush B, Newman J (**1995**) Periodic behavior in the iron/sulfuric acid system. *J Electrochem Soc* 142: 3770-3779.

[19] Sazou D (**1997**) Current oscillations and mass-transport control during electrodissolution of iron in phosphoric acid solution. *Electrochim Acta* 42: 627-637.

[20] Russell PP, Newman J (**1987**) Anodic dissolution of iron in acidic sulfate electrolytes: II. mathematical model of current oscillations observed under potentiostatic conditions. *J Electrochem Soc* 134: 1051-1059.

[21] Orazem ME, Miller MG (**1987**) The distribution of current and formation of a salt film on an iron disk below the pas,sivation potential. *J Electrochem Soc* 134: 392-399.

[22] Wang C, Chen S, Yu X (**1994**) The nature of the potentiostatic current oscillations at iron/ sulfuric acid solution interface. *Electrochim Acta* 39: 577-580.

[23] Franck UF (**1978**) Chemical oscillation. *Angew Chem Int Ed* 17: 1-15.

[24] Chen S, Wang C, Yu X (**1994**) Investigation of iron anodic process in acidic solution by holographic microphotography. *Electrochim Acta* 39: 731-736.

[25] El Rehim A, Sayed S, El Bossosi AA, El-Zien SM, Osman MM (**1994**) Electrochemical behavior of cobalt in NaOH solutions. *Collect Czech Chem Commun* 59: 2383-2389.

[26] Ibrahim MAM, Korablov SF, Yoshimura M (**2002**) Corrosion of stainless steel coated with TiN, (TiAl)N and CrN in aqueous environments. *Corros Sci* 44: 815-828.

[27] Sato N, Kuda K, Noda T (**1971**) The anodic oxide film of iron in neutral solution. *Electrochim Acta* 16: 1909-1921.

[28] Cohen M, Oswin H (**1957**) Study of the cathodic reduction of oxide films on iron: I. reduction of alpha Fe_2O_3 films. *J Electrocehm Soc* 104: 9-6.